Measuring Mass-Based Hygroscopicity of Atmospheric Particles through *in situ* Imaging

Dominique S. Piens,[1,#,] Stephen T. Kelly,[1,%] Tristan H. Harder,[1,2] Markus D. Petters,[3] Rachel E. O'Brien,[1,&] Bingbing Wang,[4,^] Ken Teske,[5] Pat Dowell,[5] Alexander Laskin,[4] Mary K. Gilles[1,*]*

[1]Chemical Sciences Division, Lawrence Berkeley National Laboratory, Berkeley, California 94720, USA

[2]Department of Chemistry, University of California, Berkeley, California 94720, USA

[3]Department of Marine Earth and Atmospheric Sciences, North Carolina State University, Raleigh, North Carolina 27695, USA

[4]William R. Wiley Environmental and Molecular Sciences Laboratory, Pacific Northwest National Laboratory, Richland, Washington 99352, USA

[5]Atmospheric Radiation Monitoring (Southern Great Plains Climate Research Facility, 109596 Coal Road, Billings, Oklahoma 74630 USA

[#]Present address: Stanford University, Stanford, California 94305, USA

[%]Present address: Carl Zeiss X-ray Microscopy Inc., Pleasanton, California 94588 USA

[&]Present address: Department of Civil and Environmental Engineering, Massachusetts Institute of Technology, Cambridge, Massachusetts 02139, USA

^Present address: College of Ocean and Earth Sciences, State Key Lab of Marine and Environmental Science, Xiamen University, Xiamen 361102, China

Keywords: aerosol water uptake, hygroscopic growth, scanning transmission X-ray microscopy, STXM, Southern Great Plains, NaCl, NaBr, $(NH_4)_2SO_4$, KCl, fructose, levoglucosan deliquescence, atmospheric aerosols, single particle, mass-based hygroscopic growth, in situ,

Manuscript submitted to

Environmental Science and Technology

ABSTRACT

Quantifying how atmospheric particles interact with water vapor is critical for understanding the effects of aerosols on climate. We present a novel method to measure the mass-based hygroscopicity of particles while characterizing their elemental and carbon functional group compositions. Since mass-based hygroscopicity is insensitive to particle geometry, it is advantageous for probing the hygroscopic behavior of atmospheric particles, which can have irregular morphologies. Combining scanning electron microscopy with energy dispersive X-ray analysis (SEM/EDX), scanning transmission X-ray microscopy (STXM) analysis, and *in situ* STXM humidification experiments, this method was validated using laboratory-generated, atmospherically relevant particles. Then, the hygroscopicity and elemental composition of 15 complex atmospheric particles were analyzed by leveraging quantification of C, N, and O from STXM, and complementary elemental quantification from SEM/EDX. We found three types of hygroscopic responses, and correlated high hygroscopicity with Na and Cl content. The mixing state determined for 158 particles broadly agreed with those of the humidified particles, indicating the potential to infer the atmospheric hygroscopic behavior from a selected subset of particles. These methods offer unique quantitative capabilities to characterize and correlate the hygroscopicity and chemistry of individual submicron atmospheric particles.

INTRODUCTION

Atmospheric aerosols affect the Earth's climate through direct effects, such as scattering and absorbing incident sunlight, and through indirect effects, where atmospheric particles interact with water vapor and act as cloud condensation or ice nuclei.[1] Their hygroscopic properties influence the uptake of volatile organics, and ultimately affect the atmospheric evolution and lifetime of particles. Quantifying how an airborne particle interacts with water vapor is critical for predicting the effect of particles on the atmospheric environment and climate, and remains an important challenge.

Multiple techniques that characterize the hygroscopic behavior of particles focus on either single-particle size measurements or the effect of water vapor on an ensemble of airborne particles.[2, 3] Frequently, in field measurements, tandem differential mobility analysis (HTDMA) is used to measure particle hygroscopicity.[4-6] With HTDMA, hygroscopic growth is quantified from changes in particle size as a function of relative humidity. However, quantifying hygroscopic growth using size is susceptible to errors due to particle asphericity and particle porosity. Additionally, inferring the hygroscopic growth of internally mixed aerosols from that of the constituent compounds may be limited by non-ideal volume additivity. Mass-based hygroscopic growth measurement provides an alternate and complimentary method to quantify water uptake.

The extent of water uptake, detailed microstructural changes of individual particles deposited on substrates, and correlation of microstructural changes with particle composition and/or chemistry during hydration/dehydration cycling can be investigated with spectromicroscopy. Spectromicroscopic methods include micro-FTIR,[7, 8] micro-Raman,[9-11] micro-Raman combined with atomic force microscopy,[12] scanning and transmission electron

70 microscopy with energy dispersive analysis of X-rays (SEM/EDX),[13-15] and scanning
71 transmission X-ray microscopy with near-edge X-ray absorption fine structure spectroscopy
72 (STXM/NEXAFS).[16] These are used to examine particle efflorescence and deliquescence,[17]
73 changes in morphology,[18] water vapor uptake,[19] and liquid-liquid phase separation.[20-22]
74 STXM/NEXAFS is uniquely capable of quantitative analysis of the light elements (C, N, O)
75 while probing their chemical bonding at spatial resolution down to 25 nm.[16, 23-25] Several groups
76 have employed chemical imaging by STXM/NEXAFS under controlled water vapor
77 environment.[18, 26-30] These include qualitative observations of hygroscopic properties in humic
78 like substances (HULIS) as proxies for aerosols,[30] atmospheric particles collected from the
79 Amazonian basin,[18] deliquescence and efflorescence of laboratory generated particles,[27, 29] and
80 quantitative measurements of water content in single-component proxies of atmospheric
81 particles.[26, 31]

82 Here, a methodology is presented to quantify mass-based water uptake in individual
83 submicron particles that combines STXM/NEXAFS particle characterization with *in situ* and
84 water vapor uptake measurements complemented with subsequent SEM/EDX elemental
85 composition microanalysis. The utility of *in situ* STXM/NEXAFS chemical imaging for mass-
86 based water vapor uptake measurements is demonstrated using laboratory-generated particles of
87 known compositions and uniform morphologies. Field samples, collected from the Department
88 of Energy's Atmospheric Radiation Monitoring (DOE-ARM) site in the Southern Great Plains
89 (SGP) field site, are then examined. For STXM/NEXAFS measurements, the dry particle
90 composition was characterized before the sample was subjected to *in situ* water vapor uptake
91 experiments. Subsequently, SEM/EDX elemental characterization of the identical particles was
92 performed. Finally, a composition analysis combined the STXM/NEXAFS and SEM/EDX data

sets to determine mass-based hygroscopicity parameters for the atmospheric particles collected at the SGP site. This is the first application combining these microscopic techniques to determine total mass of individual particles both for the laboratory generated as well as field samples. The use of mass rather than size to track hygroscopic growth enabled the extension of established methods to atmospheric particles. A brief discussion on the future outlook for utilizing this analysis to extract mass-based hygroscopicity parameters from any complex heterogeneous population of atmospheric particles is presented.

EXPERIMENTAL SECTION

Laboratory Particle Preparation. Particles composed of NaCl, NaBr, $(NH_4)_2SO_4$, KCl, fructose, and levoglucosan were prepared by nebulizing (nebulizer, Stalter Labs, model 8900) a dilute solution (0.5 M) of stock chemical in deionized H_2O (18 MΩ resistivity). Particles then passed through a diffusion dryer, and were collected onto Si_3N_4 substrates on the 7th stage (D_{50} = 0.56 μm) of a Multi-Orifice Uniform Deposition Impactor (MOUDI; model 110-R, MSP, Inc.). To dry and recrystallize the particles, the substrates were baked at ~80 °C in ambient atmosphere for several days and then stored in a desiccator until use (several days-months).

Atmospheric Particle Collection. Atmospheric particles were collected at the DOE-ARM SGP sampling site in Oklahoma, USA on March 27th 2014 at 19:00 GMT. Particle samples were collected for 20 minutes using a 4-stage Sioutas cascade impactor operated at a flow rate of 9 L/min. Each stage was preloaded with silicon nitride membrane substrates (0.5 × 0.5 mm^2 Si_3N_4 window size, 100 nm membrane thickness, 5 × 5 mm^2 Si frame size; Silson, Inc.) and filmed TEM grids (Carbon type B film, Copper 400 mesh grids; Ted Pella, Inc.). The samples collected on the fourth stage (D_{50} = 0.25 μm) were used for microscopy analysis. After collection,

116 the samples were placed in sealed containers, transported, and then stored in a desiccator (20-30
117 % relative humidity) until STXM analysis (two weeks later). Between subsequent experiments
118 (water vapor uptake, SEM/EDX, additional STXM analysis) over the following 6 months, the
119 samples were stored in a sealed package in a desiccator.
120 **STXM/NEXAFS Measurements.** STXM/NEXAFS was used to characterize the dry
121 laboratory and field samples. The measurements were performed at beamline 11.0.2 of the
122 Advanced Light Source at Lawrence Berkeley National Laboratory. Details of the STXM
123 instrument and its operation are described elsewhere,[32] its applications for analysis of
124 atmospheric particles are described in a recent review,[16] and additional details on these
125 experiments as well as nitrogen analysis are included in the Supporting Information (SI) file.
126 Briefly, in STXM experiments, monochromatic light from the synchrotron is focused to a small
127 (25-40 nm) spot at the sample location by a Fresnel zone plate lens. The sample is raster scanned
128 through the focused beam while the transmitted X-rays are collected on a single element detector
129 behind the sample to create an image. By changing the X-ray energy, the image contrast can be
130 changed to highlight particular molecular bonds and functional groups. Collecting the same
131 image at different X-ray energies spanning across an elemental absorption (referred to
132 collectively as a *stack*) allows data acquisition for spatially resolved NEXAFS spectroscopy.
133 Specific energies are then selected to acquire "short stacks" at a reduced number of energies.
134 These "short stacks" allow more rapid mapping of carbon functional groups to allow data
135 acquisition on a larger number of particles within the limited beamtime. Here, the number of data
136 points collected at the C, N, and O pre-edge and post-edge energies is larger than previously
137 used.[33] In samples containing a significant fraction of inorganic constituents, this allows a more
138 precise fitting of the fall off of the absorption cross section, using the Henke functions[34] to

139 constrain the inorganic mass. The presence of an element is quantitatively *mapped* by comparing
140 an image collected either in the post-edge region (~25-30 eV beyond the elemental absorption
141 edge for elemental mapping) or at a particular molecular resonance (to map chemical bonding) to
142 an image collected in the pre-edge region ~15-20 eV below the energy where the element
143 absorbs. Additional details are provided in the SI.

144 **Characterization of Laboratory Generated Particles**. Samples of laboratory-generated
145 particles were directly loaded in the micro reactor used for the water vapor uptake experiments.
146 Prior to humidification, STXM/NEXAFS oxygen maps of individual dry submicron particles
147 confirmed the absence of oxygen in NaCl, NaBr, and KCl, laboratory generated samples,
148 indicating that they were free of water. For these salt particles as well as $(NH_4)_2SO_4$, carbon data
149 was not acquired. For fructose and levoglucosan, both carbon short stacks and oxygen maps were
150 collected prior to water vapor exposure.

151 **Characterization of Particles from the Southern Great Plains.** To ascertain how
152 representative the particles used for the water vapor uptake experiments were, prior to
153 humidification experiments, 158 additional particles from the field sample were analyzed. The
154 STXM/NEXAFS stacks of particles from SGP field samples at the carbon K-edge provided
155 information on their chemical composition and allowed a mixing state classification based on the
156 amounts of organic carbon (OC), sp^2-hybridized carbon (an indicator of soot or elemental
157 carbon, EC), and inorganic species (IN).[33] For the mixing state determination, values for the
158 optical density across the carbon edge for every pixel allowed an analysis of the chemical
159 composition on a pixel-by-pixel basis. After analyzing the individual pixels, a compositional
160 map of each particle was generated. Particles can contain mixtures of the three components
161 organic (OC), inorganic (IN), and black carbon/soot (EC), additional analysis details are

provided in Moffet et al.[33] The STXM particle mixing state was classified as organic carbon (OC), organic and elemental carbon (OCEC), organic and elemental carbon as well as inorganics (OCECIN) or organic carbon with inorganics (OCIN).[33]

***In Situ* STXM/NEXAFS Water Vapor Uptake Measurements**. The micro-reactor, described in Kelly et al.,[27] was used for *in situ* STXM/NEXAFS chemical imaging of particles exposed to controlled relative humidity (RH). Two helium gas flows with a combined flow rate of 6 sccm, one saturated with water vapor and the other dry, were used to control RH inside the reactor. A sensor (GE Chipcap-L), located in the reactor, measured RH and temperature inside the reactor. A SiN_x window with a sample of impacted particles is mounted to the removable metal faceplate using a small amount of wax (Crystalbond 509, SPI Supplies). Since the wax must be heated to be applied to the SiN_x window, impacted aerosols are exposed to a maximum temperature of up to 50-70 °C for 15-30 seconds during mounting.

After 158 particles were characterized using a higher resolution zone plate (25 nm) for total inorganic content, carbon, and oxygen, the sample was loaded in the micro reactor for the water vapor uptake experiments. Due to geometrical constraints discussed in Kelly et al.,[27] the water vapor uptake experiments used a 40 nm Fresnel zone plate. Three sample regions, containing particles with compositions and morphologies representative of those in the initial characterization of 158 particles, and with sufficient spacing between particles (to limit coalescence during hygroscopic growth) were selected for water vapor uptake experiments. For each of these regions, carbon short stacks and oxygen maps were collected under dry (<4 % RH) conditions with 40 nm lateral resolution.

The RH was then increased stepwise (steps of 5-10 % RH) and stabilized for 5-10 minutes before each set of data acquisition. At each RH step, oxygen maps were collected to

quantify changes in the particle oxygen content attributed to water uptake. After reaching the maximum RH, the RH was decreased (steps of 10-20% RH) and stabilized for 5-10 minutes prior to collecting oxygen maps. The total number of single-energy images acquired on each region was ~120. Hence, the soft X-ray irradiation was minimized and similar to that typical of a single carbon full stack. Pattern matching with the positions and morphologies of impacted aerosols allowed rapid relocation of the identical particles for subsequent SEM/EDX analysis.

SEM/EDX Measurements. After the STXM/NEXAFS water vapor uptake experiments, the identical particles were relocated and imaged for elemental composition using SEM/EDX. An FEI Quanta digital field emission gun environmental scanning electron microscope was used in this work. The microscope is equipped with an EDAX X-ray spectrometer with a Si(Li) detector with an active area of 10 mm^2 and an ATW2 window. X-ray spectra were acquired for the same individual particles probed in the STXM experiments for 10 s, at a beam current of 430 pA and an accelerating voltage of 20 kV. Elements considered in the X-ray analysis were Na, Mg, Al, P, S, Cl, K, Ca, Mn, Fe, and Zn. Individual particle EDX spectra were pre-processed removing elements having less than 0.5 atomic %. Additional details of the SEM/EDX analysis of deposited particles deposited are found in Laskin et al.[15] and references therein.

Data Processing and Analysis. The analytical techniques, applications, and limitations of the mapping and quantitative chemical imaging of particle samples by STXM are presented elsewhere[16] and only briefly discussed here. Data analysis is performed using MATLAB (Mathworks, Natick, MA). Two-dimensional transmission intensity images are obtained by raster-scanning samples of impacted particles in the STXM. In each image, the background intensity value (I_0) is determined from substrate areas without particles. I_0 is used to convert transmission intensity into optical density, (OD) units of absorption using Beer's law. This

208 analysis required additional MATLAB scripts beyond those in Moffet et al.[33] To identify image
209 areas corresponding to individual particles, masks were manually drawn around particles.
210 Individual particles at different RH values were matched visually. For each particle and RH,
211 particle mass, m, was calculated using

212 $$m = \frac{\sum_i OD_i \cdot S}{\mu} \qquad (1)$$

213 where i is a pixel in a particle's image, OD_i is the absorption at the i-th pixel at a given X-ray
214 energy, m is the particle mass, and S is the area of a pixel. The particle's mass-absorption cross
215 section, μ, is based on the particle's average elemental composition, and calculated using

216 $$\mu = \frac{\sum_j x_j A_j \mu_j}{\sum_j x_j A_j} \qquad (2)$$

217 where x_j is the atomic fraction of element j, A_j, is the molar mass of element j, and μ_j, is the mass-
218 absorption cross section of element j at the specific X-ray energy.[34] OD at the X-ray energies of
219 an element's X-ray absorption edge and the mass-absorption cross section of that element are
220 used in eq. 1 to obtain the mass of a given element in a particle.
221 Dry particle masses (~4% RH) and masses of the particle plus condensed water were
222 calculated using these formulas and used to derive mass-based growth factors. This step is
223 analogous to that employed by Ghorai and Tivanski.[26] For laboratory-generated particles
224 containing oxygen, the dry mass is determined with eq 1 at the oxygen pre-edge using their
225 known chemical formula. Laboratory-generated aerosols without oxygen (i.e. NaCl and other
226 salts) were calculated with no dry oxygen mass (confirmed with STXM/NEXAFS imaging). To
227 obtain the mass of the condensed water, the total oxygen mass was calculated using eq 1 at the
228 oxygen post-edge. For oxygen-containing particles (fructose, levoglucosan, and ammonium
229 sulfate), water mass at each RH is obtained by subtracting the initial dry oxygen mass, from the

total oxygen mass to obtain the condensed water mass (m_w). Dry total mass (m_s) and m_w yield a mass-based growth factor at every RH (g_m).

$$g_m = \frac{m_s + m_w}{m_s} \qquad (3)$$

Total Masses from STXM/NEXAFS and SEM/EDX: Atmospheric Particles of Unknown Composition. STXM/NEXAFS measurements of C, N, and O were combined with the SEM/EDX measurements for high-Z elements to calculate the total mass of dry individual particles. In STXM/NEXAFS the sum of the OD over all pixels of a given particle is proportional to the mass-absorption cross section of the average composition of the particle, and to its total mass (eq 1). Total OD for elements other than C, N, and O is obtained by summation over a particle's STXM/NEXAFS image pixels at 278 eV (the carbon, nitrogen, and oxygen *K* pre-edges). An empirical formula for the average composition of a particle is obtained by summing its spatially resolved atomic fractions of the most common elements of Al, Ca, Cl, Fe, K, Mg, Mn, Na, P, S, and Zn measured with SEM/EDX. SEM/EDX is quantitative[15] for these elements and they represent the majority of particle inorganic mass. A mass-absorption cross section, calculated from the empirical formula using eq 2, is used in eq 1 to obtain the total inorganic mass. Si was excluded because the sample substrate contains silicon. The uncertainty due to this is discussed in the SI file as well as additional information on the nitrogen content (Figure S1 and related discussion). Carbon, nitrogen, and oxygen masses obtained from STXM/NEXAFS were added to the inorganic mass determined with SEM/EDX to obtain the total mass of each individual dry particle.

RESULTS AND DISCUSSION

Hygroscopic Behavior of Laboratory-Generated Samples with Known Composition. In Figure 1, experimental values of the mass-based growth factor (g_m) as a

function of RH obtained from STXM/NEXAFS, represented by triangles, are compared to values predicted by the thermodynamic model AIOMFAC, shown as solid black lines.[35, 36] Dashed black lines indicate the sorption isotherm of idealized crystalline salts. Prior to deliquescence, hygroscopic growth is negligible. At deliquescence, hygroscopic growth appears as a step to the g_m, as predicted by AIOMFAC. Data on the mass-based growth factors for laboratory generated samples as a function of relative humidity is provided in the Supporting Information Tables S1-S4.

Generally, the salts (Fig. 1 a-d) follow idealized crystalline growth until their deliquescence RH (DRH), and after their DRH, agree with AIOMFAC. KCl (Fig. 1c) and ammonium sulfate (Fig. 1d) further support that trend in hygroscopic behavior because the hysteresis during their dehydration resembles the growth of aqueous particles modeled by AIOMFAC. Due to limited instrumental access, values for g_m were not obtained during dehydration for the other lab-generated samples or above DRH. The DRH observed for NaBr is consistent with those reported by Cohen et al. (between 44.5% and 45.5%)[37] and Wise et al. (between 46% and 47%) .[38] For NaBr, the value of g_m jumps from 1.1 at 47% RH to 1.6 at 49% RH. Within the RH measurement uncertainty of 2%[27] the measured DRH of the crystalline salts are in agreement with literature values.

Unlike crystalline salts, which exhibit sharp deliquescence phase transition, levoglucosan and fructose exhibit gradual hygroscopic growth. For levoglucosan, as previously observed by Mikhailov et al.[39] and Mochida and Kawamura,[40] g_m increases with higher RH more rapidly than a UNIFAC-based model predicts. AIOMFAC uses UNIFAC group contribution methods to predict activity coefficients and hygroscopic behavior. Mochida and Kawamura[40] proposed that UNIFAC interaction coefficients were not optimized for organic molecules containing a high

ratio of polar groups to nonpolar groups or closely-spaced polar groups such as levoglucosan. The sorption isotherm for fructose also exhibits higher growth at high RH than predicted by AIOMFAC.

The difference between AIOMFAC and experimental values could partially be explained by a combination of our methods estimating lower initial particle mass and higher water mass at high RH than AIOMFAC. Given their continuing hygroscopic growth, sugar particles were amorphous rather than crystalline. Although the sugar particles were gently dried at 80˚C over several hours or overnight, they may have contained trace residual water and been highly viscous. Mikhailov et al. suggested that this scenario could lead to higher observed g_m values at high RH since the observed initial particle mass will be lower than the theoretical one due to water adsorption being surface limited.[39] Therefore, differences between model assumptions and experimental conditions could explain some of the deviations in the g_m of sugars at high RH between experiment and AIOMFAC. Future experiments measuring the hygroscopic growth of lab-generated organic particles containing traces of inorganics would approximate atmospheric particles more closely, and reveal how differences between AIOMFAC and experiment impact our methods for atmospheric particles. Overall, these methods measure the hygroscopic response of individual particles of known composition in agreement with AIOMFAC.

Hygroscopic Behavior of Atmospheric Aerosol Samples of Unknown Composition.

This is the first time STXM/NEXAFS and SEM/EDX are combined to determine mass-based growth factors for field collected atmospheric particles. This combination leverages the strengths of each technique and enables accurate determination of particle mass and adsorbed water mass, while also spatially identifying prominent organic chemical functional groups within individual particles.

Figure 2 depicts the range of characteristic hygroscopic curves measured for complex individual atmospheric particles containing both organic and inorganic components. Particles cluster into three types of hygroscopic responses labeled as low, medium, and high hygroscopicity particles. Mass-based growth factors as a function of relative humidity for these three types are provided in the Supporting Information Tables S5-S7.

The size-based growth factors of the atmospheric particles (Figure S2 and Table S9, Supporting Information) yield very different growth curves. In contrast to mass-based hygroscopic growth, the particles do not cluster by type based on size growth factors obtained from their area equivalent diameter. Additionally, the 2D projections for some particles even decrease with increased water uptake. Hence, the findings in this manuscript are only observable using mass-based growth factors rather than size-based growth factors.

Complementary, STXM/NEXAFS can quantify C, N, and O content and water uptake, while SEM/EDX can quantify inorganic elements on a single-particle basis. Figure 3 shows atomic fractions of inorganic elements for low, medium, and high hygroscopicity particles. A single correlation was found between the composition of the inorganic fraction of particles and the hygroscopic response of particles. High hygroscopicity particles have higher atomic fractions of Na and Cl than medium and low hygroscopicity particles. The water sorption isotherm of lab-generated NaCl is shown with the water sorption isotherm of the high hygroscopicity particles in Figure 2. The plot emphasizes that high hygroscopic growth occurs between 72% and 78% RH for high hygroscopicity particles, very near NaCl DRH (75.3% RH). Laboratory-generated NaCl and high hygroscopicity particles have similar discontinuities in hygroscopic growth. This suggests that Na and Cl in the form of NaCl may drive the hygroscopic growth of high

hygroscopicity particles. Atomic fractions for the other elements show significant overlap between particles with different hygroscopicities.

To provide an alternate representation of the hygroscopicity of the atmospheric particles, another parameter representing aerosol-water interactions is presented in Figure 3. Petters and Kreidenweis introduced the use of a single parameter, κ, to represent the effect a particle has on water activity by calculating the ratio of the volume of water to particulate matter.[42] Higher values of κ correspond to higher hygroscopicity and for atmospherically relevant particles κ typically ranges from 0 to values exceeding 1. However, instead of a ratio of volumes mass-based growth factors can also be used to calculate κ by assuming particle density. A density-equivalent κ_{equiv}, which is defined as the κ value of a particle with the observed hygroscopic mass growth factor and assumed dry density, ρ_d, is calculated with equation 4:

$$\kappa_{equiv} = (a_w^{-1} - 1)(g_m - 1)r \quad (4)$$

where r is the ratio of dry particle density to the density of pure water. Here we assume r = 1.760 based on the density of solid ammonium sulfate. Kelvin effects are neglected and water activity is taken to be the equilibrium RH. Density equivalent κ provides an approximate comparison to volume-growth factor published data in the literature.[42-44] If the studied particle density equals that of assumed value, the reported κ_{equiv} is identical to κ obtained via volumetric methods. A 10% relative difference between actual and assumed particle density results in a 10% difference to values inferred from the volumetric-based method. The density equivalent κ_{equiv} values can be compared to the known κ values of other substances.[42-44] In this study, the most hygroscopic atmospheric particle observed has a density equivalent κ_{equiv} of 0.71 at high RH (80%), which is much lower than the estimated κ_{equiv} value reported for NaCl, but near the estimated κ_{equiv} values for most sulfate and nitrate salts typically found in atmospheric aerosols.[41] Medium and low

hygroscopicity particles have κ_{equiv} values in the same range as organic particles, attaining the lowest possible value of 0 for the low hygroscopicity particles.[42]

As described above, STXM/NEXAFS at the carbon K-edge identifies three components: organic (OC), inorganic (IN), and black carbon/soot (EC) to define a mixing state.[33] Figure S3 in the Supporting Information contains images that illustrate how the mixing state is determined for particles and Table S8 provides details on the mixing state classification. Figure 4 (left panel) shows the STXM based mixing states of the particles used for hygroscopic growth experiments (green) compared to that of the sample of 158 particles (blue). Based upon a visual analysis of preliminary STXM images we anticipated that these 15 particles were reasonably representative of the samples. Hence, they were selected for water vapor uptake experiments. Figure 4 (right panel) compares the size distribution of the 158 particles characterized using STXM/NEXAFS (blue) compared to that of the 15 particles selected for water vapor uptake experiments (green). Overall, the particle size distributions match well between the two sample sets. The agreement for the mixing state is slightly lower (Figure 4, left panel) indicating that field samples containing more diverse particle-types would require better statistical depth. With the sample size of 15 particles, no significant correlation was found between hygroscopicity, and mixing state or particle size. However, if correlations were observed, by using a statistically significant subset of the population, then estimates for the hygroscopic behavior of the sample could be obtained. Additional characterization of the IN, via analysis with SEM/EDX, would be required as kappa values vary for different inorganic compounds.[42]

STXM/NEXAFS has previously been used to quantify the hygroscopicity of laboratory generated particles of known composition[26, 27, 29, 30] and to observe the hygroscopic behavior of ambient particles of unknown composition.[18] Here, we demonstrated that the combination of

STXM/NEXAFS and SEM/EDX could quantitatively determine the hygroscopic behavior of both homogeneous particles with known composition and mixed atmospheric particles of unknown composition. Mass-based growth factors of mixed atmospheric particles of unknown composition were obtained on a per-particle basis by combining SEM/EDX measurements with STXM/NEXAFS characterizations. This method was validated using laboratory surrogates. Such data on field samples may provide means to correlate hygroscopic behavior and particle composition and chemistry. Although we attempted to find correlations between carbon functional groups (C=C, R-OH, COOH) and particle hygroscopicity, no apparent relationship was found. The mass-based growth factors can be used to characterize the statistics and range of hygroscopic behavior present in a sample of collected atmospheric particles and relate this range of behavior to elemental and functional chemistry.

ASSOCIATED CONTENT

Supporting Information

More detailed experimental methods for STXM/NEXAFS measurements and the characterization of SGP samples; the effects of uncertainty in nitrogen and silicon measurements on the mass-based growth factors of the SGP atmospheric particles; plot of size-based growth factors as a function of RH for the SGP atmospheric particles; tables containing the experimental data displayed in figures 1-4; images illustrating the mixing state of particles in terms of OC, EC and IN. This material is available free of charge via the Internet at http://pubs.acs.org.

AUTHOR INFORMATION

Corresponding Authors

*E-mail: dpiens@stanford.edu

*E-mail: mkgilles@lbl.gov

ACKNOWLEDGEMENTS

STXM/NEXAFS dry characterization experiments (MKG, STK, THH) were supported by the Atmospheric Systems Research (ASR) of the U.S. Department of Energy (DOE), Office of Science, Office of Biological and Environmental Research (OBER) program. Dry STXM/NEXAFS analysis of the field samples (THH) was partially supported by the German National Academic Foundation. Development of the MATLAB scripts and analysis for the mass-based water vapor uptake analysis (DSP) was supported through the DOE, Office of Workforce Development for Teachers and Scientists (WDTS) under the Science Undergraduate Laboratory Internship (SULI) program. REO (supported by DOE ASR) provided analysis guidance to both DSP and THH. The experimental portion of the water vapor uptake experiments (STK, MKG) and assistance with the interpretation of the data (MP) was supported by the ASR DOE OBER program. STXM/NEXAFS measurements were done with the assistance of Tolek Tyliszczak at Beamline 11.0.2 of the Advanced Light Source (ALS) at Lawrence Berkeley National Laboratory (LBNL). The ALS is supported by the Director, Office of Science, Office of Basic Energy Sciences (BES), of the U.S. DOE under Contract No. DE-AC02-05CH11231. Beamline 11.0.2 is supported under the same contract as well as the Condensed Phase and Interfacial Molecular Sciences Program of DOE BES. AL and BW acknowledge support from support from the Chemical Imaging Initiative of the Laboratory Directed Research and Development program at Pacific Northwest National Laboratory (PNNL). The preparation of laboratory samples and SEM/EDX measurements were performed at the W. R. Wiley Environmental Molecular Sciences Laboratory (EMSL) - a national scientific user facility located at PNNL, and sponsored by DOE OBER. PNNL is operated for US DOE by Battelle Memorial Institute under Contract

413 No. DE-AC06-76RL0 1830. Samples were collected (KT, PD) at the Atmospheric Radiation
414 Monitoring (ARM) site located at Southern Great Plains and sponsored by DOE OBER.

TOC Art

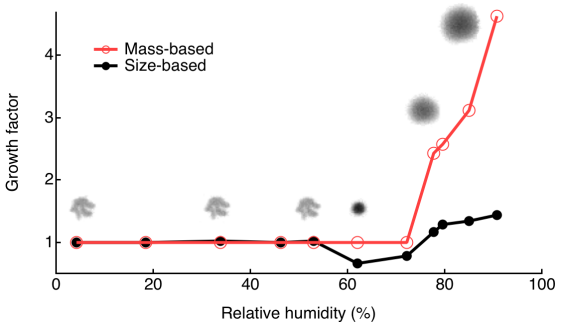

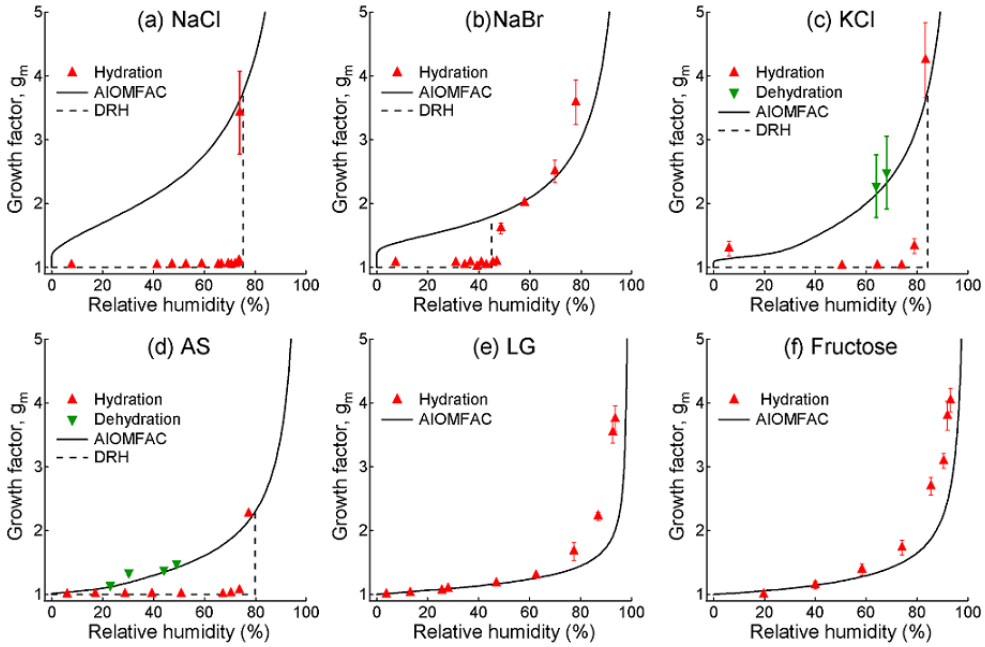

Figure 1. Experimental (red filled triangles) and AIOMFAC theoretical (black lines) mass-based growth factors as a function of relative humidity for (a) NaCl, (b) NaBr, (c) KCl, (d) $(NH_4)_2SO_4$ labeled AS, (e) levoglucosan labeled LG, and (f) fructose. Dehydration data points are shown as green filled triangles. Deliquescence relative humidities (DRH) for NaCl and ammonium sulfate were obtained from Tang[43] and NaBr and KCl are from Cohen et al.[37]

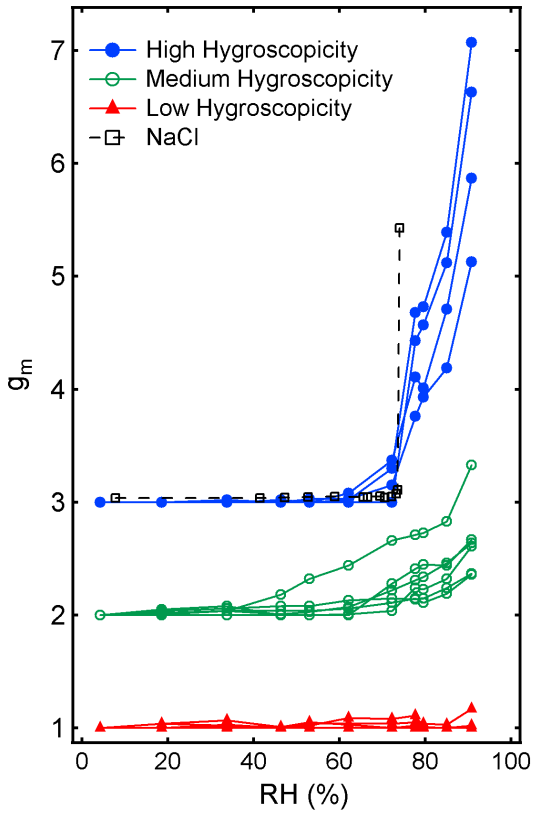

Figure 2. Mass-based growth factors of individual atmospheric aerosols (offset for clarity: by 1 for the green and 2 for the blue data points) grouped by their hygroscopic growth regime as a function of relative humidity. The water sorption isotherm of NaCl is overlaid on the water sorption isotherm of high hygroscopicity atmospheric aerosols.

Particle #	Hygroscopicity	g_m at 80% RH	NaCl Equivalent κ	Inorganic Atomic Fractions	4% RH	90% RH	Mixing State
1	High	2.73	0.71				OCIN
2	High	2.57	0.64				OCIN
3	High	2.01	0.41				OCECIN
4	High	1.93	0.38				OCIN
5	Medium	1.73	0.30				OCIN
6	Medium	1.45	0.18				OCECIN
7	Medium	1.34	0.14				OCIN
8	Medium	1.23	0.09				OCECIN
9	Medium	1.15	0.06				OCECIN
10	Medium	1.11	0.05				OCECIN
11	Low	1.04	0.02				OCECIN
12	Low	1.01	0.00				OCIN
13	Low	1.00	0.00				OCEC
14	Low	1.00	0.00				OCECIN
15	Low	1.00	0.00				OCECIN

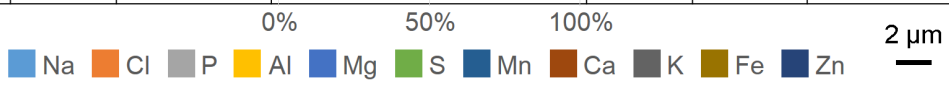

Figure 3. Table presenting hygroscopicity, mass-based growth factor at 80% RH (g_m), inorganic atomic composition, STXM images at 4% and 90% RH acquired at 525 eV, and mixing state classification for 15 atmospheric particles.

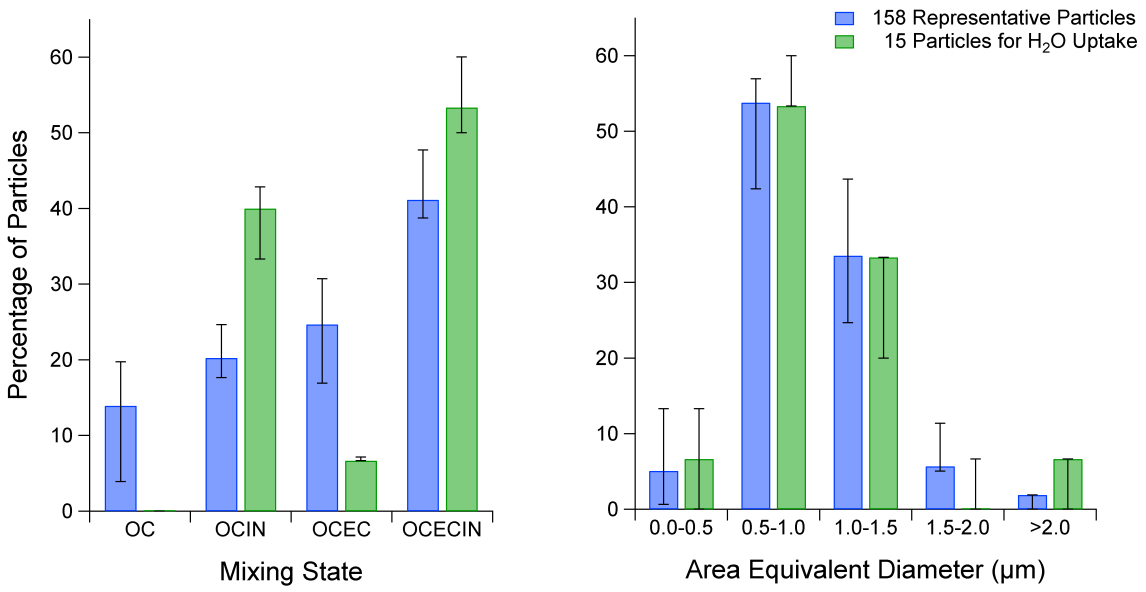

Figure 4. Left: STXM based mixing state distribution of all particles characterized on the Southern Great Plains sample (158) and the subset of the 15 particles used during water vapor uptake experiments. Mixtures of individual components (organic (OC), inorganic (IN), and black carbon/soot (EC)) within individual particles are indicated. Error bars calculated by varying the detection thresholds of the individual components by 10% are shown. Right: the corresponding size distributions. The error bars represent the effect of an estimated uncertainty of ± 2 pixels on the bar classification of the two particle groups.

REFERENCES

1. Andreae, M. O.; Rosenfeld, D., Aerosol-cloud-precipitation interactions. Part 1. The nature and sources of cloud-active aerosols. *Earth-Sci. Rev.* **2008,** *89*, (1-2), 13-41. DOI 10.1016/J.Earscirev.2008.03.001
2. Nguyen, T. K. V.; Petters, M. D.; Suda, S. R.; Guo, H.; Weber, R. J.; Carlton, A. G., Trends in particle-phase liquid water during the Southern Oxidant and Aerosol Study. *Atmos. Chem. Phys.* **2014,** *14*, (20), 10911-10930. DOI 10.5194/Acp-14-10911-2014
3. Swietlicki, E.; Hansson, H. C.; Hameri, K.; Svenningsson, B.; Massling, A.; McFiggans, G.; McMurry, P. H.; Petaja, T.; Tunved, P.; Gysel, M.; Topping, D.; Weingartner, E.; Baltensperger, U.; Rissler, J.; Wiedensohler, A.; Kulmala, M., Hygroscopic properties of submicrometer atmospheric aerosol particles measured with H-TDMA instruments in various environments - a review. *Tellus B* **2008,** *60*, (3), 432-469. DOI 10.1111/J.1600-0889.2008.00350.X
4. Suda, S. R.; Petters, M. D., Accurate determination of aerosol activity coefficients at relative humidities up to 99% using the hygroscopicity tandem differential mobility analyzer technique. *Aerosol. Sci. Tech.* **2013,** *47*, (9), 991-1000. DOI 10.1080/02786826.2013.807906
5. Yeung, M. C.; Lee, B. P.; Li, Y. J.; Chan, C. K., Simultaneous HTDMA and HR-ToF-AMS measurements at the HKUST Supersite in Hong Kong in 2011. *J. Geophys. Res.-Atmos.* **2014,** *119*, (16), 9864-9883. DOI 10.1002/2013jd021146
6. Martin, S. T.; Rosenoern, T.; Chen, Q.; Collins, D. R., Phase changes of ambient particles in the Southern Great Plains of Oklahoma. *Geophys. Res. Lett.* **2008,** *35*, (22). DOI 10.1029/2008GL035650
7. Liu, Y.; Laskin, A., Hygroscopic properties of CH_3SO_3Na, CH_3SO_3NH4, $(CH_3SO_3)_2Mg$, and $(CH_3SO_3)_2Ca$ particles studied by micro-FTIR spectroscopy. *J. Phys. Chem. A.* **2009,** *113*, (8), 1531-1538. DOI 10.1021/Jp8079149
8. Liu, Y.; Yang, Z.; Desyaterik, Y.; Gassman, P. L.; Wang, H.; Laskin, A., Hygroscopic behavior of substrate-deposited particles studied by micro-FT-IR spectroscopy and complementary methods of particle analysis. *Anal. Chem.* **2008,** *80*, (3), 633-642. DOI 10.1021/Ac701638r
9. Ciobanu, V. G.; Marcolli, C.; Krieger, U. K.; Weers, U.; Peter, T., Liquid-liquid phase separation in mixed organic/inorganic aerosol particles. *J. Phys. Chem. A.* **2009,** *113*, (41), 10966-10978. DOI 10.1021/jp905054d
10. Yeung, M. C.; Chan, C. K., Water content and phase transitions in particles of inorganic and organic species and their mixtures using micro-Raman spectroscopy. *Aerosol. Sci. Tech.* **2010,** *44*, (4), 269-280. DOI 10.1080/02786820903583786
11. Garland, R. M.; Wise, M. E.; Beaver, M. R.; DeWitt, H. L.; Aiken, A. C.; Jimenez, J. L.; Tolbert, M. A., Impact of palmitic acid coating on the water uptake and loss of ammonium sulfate particles. *Atmos. Chem. Phys.* **2005,** *5*, 1951-1961.
12. Laskina, O.; Morris, H. S.; Grandquist, J. R.; Qin, Z.; Stone, E. A.; Tivanski, A. V.; Grassian, V. H., Size matters in the water uptake and hygroscopic growth of atmospherically relevant multicomponent aerosol particles. *J. Phys. Chem. A* **2015,** *119*, (19), 4489-97. DOI 10.1021/jp510268p
13. Laskin, A., Electron beam analysis and microscopy of individual particles. In *Fundamentals and Applications in Aerosol Spectroscopy*, Signorell, R.; Reid, J. P., Eds. CRC Press Taylor & Francis: Boca Raton, FL., 2010; pp 463-491.

14. Posfai, M.; Buseck, P. R., Nature and climate effects of individual tropospheric aerosol particles. *Annu. Rev. Earth Pl. Sc.* **2010,** *38*, 17-43. DOI 10.1146/Annurev.Earth.031208.100032
15. Laskin, A.; Cowin, J. P.; Iedema, M. J., Analysis of individual environmental particles using modern methods of electron microscopy and X-ray microanalysis. *J. Electron Spectrosc. Relat. Phenom.* **2006,** *150*, (2-3), 260-274. DOI 10.1016/j.elspec.2005.06.008
16. Moffet, R. C.; Tivanski, A. V.; Gilles, M. K., Scanning transmission X-ray microscopy: Applications in atmospheric aerosol research. In *Fundamentals and Applications in Aerosol Spectroscopy*, Signorell, R.; Reid, J. P., Eds. CRC Press Taylor & Francis: Boca Raton, FL., 2010; pp 420-462.
17. Freney, E. J.; Martin, S. T.; Buseck, P. R., Deliquescence and efflorescence of potassium salts relevant to biomass-burning aerosol particles. *Aerosol. Sci. Tech.* **2009,** *43*, (8), 799-807. DOI 10.1080/02786820902946620
18. Pöhlker, C.; Saturno, J.; Kruger, M. L.; Forster, J. D.; Weigand, M.; Wiedemann, K. T.; Bechtel, M.; Artaxo, P.; Andreae, M. O., Efflorescence upon humidification? X-ray microspectroscopic in situ observation of changes in aerosol microstructure and phase state upon hydration. *Geophys. Res. Lett.* **2014,** *41*, (10), 3681-3689. DOI 10.1002/2014gl059409
19. Ghorai, S.; Wang, B. B.; Tivanski, A.; Laskin, A., Hygroscopic properties of internally mixed particles composed of NaCl and water-soluble organic acids. *Environ. Sci. Technol.* **2014,** *48*, (4), 2234-2241. DOI 10.1021/Es404727u
20. You, Y.; Renbaum-Wolff, L.; Carreras-Sospedra, M.; Hanna, S. J.; Hiranuma, N.; Kamal, S.; Smith, M. L.; Zhang, X. L.; Weber, R. J.; Shilling, J. E.; Dabdub, D.; Martin, S. T.; Bertram, A. K., Images reveal that atmospheric particles can undergo liquid-liquid phase separations. *Proc. Natl. Acad. Sci. U. S. A.* **2012,** *109*, (33), 13188-13193. DOI 10.1073/pnas.1206414109
21. You, Y.; Smith, M. L.; Song, M. J.; Martin, S. T.; Bertram, A. K., Liquid-liquid phase separation in atmospherically relevant particles consisting of organic species and inorganic salts. *Int. Rev. Phys. Chem.* **2014,** *33*, (1), 43-77. DOI 10.1080/0144235x.2014.890786
22. O'Brien, R. E.; Wang, B.; Kelly, S. T.; Lundt, N.; You, Y.; Bertram, A. K.; Laskin, A.; Gilles, M. K., Imaging of liquid-liquid phase separation in aerosol particles at nanometer scale. *Env. Sci. Technol.* **2015,** *49*, 4995-5002. DOI 10.1021/acs.est.5b00062
23. Tivanski, A. V.; Hopkins, R. J.; Tyliszczak, T.; Gilles, M. K., Oxygenated interface on biomass burn tar balls determined by single particle scanning transmission X-ray microscopy. *J. Phys. Chem. A.* **2007,** *111*, (25), 5448-5458. DOI 10.1021/Jp070155u
24. Hopkins, R. J.; Tivanski, A. V.; Marten, B. D.; Gilles, M. K., Chemical bonding and structure of black carbon reference materials and individual carbonaceous atmospheric aerosols. *J. Aerosol Sci.* **2007,** *38*, (6), 573-591. DOI 10.1016/j.jaerosci.2007.03.009
25. Maria, S. F.; Russell, L. M.; Gilles, M. K.; Myneni, S. C. B., Organic aerosol growth mechanisms and their climate-forcing implications. *Science* **2004,** *306*, (5703), 1921-1924. DOI 10.1126/Science.1103491
26. Ghorai, S.; Tivanski, A. V., Hygroscopic behavior of individual submicrometer particles studied by X-ray spectromicroscopy. *Anal. Chem.* **2010,** *82*, (22), 9289-9298. DOI 10.1021/Ac101797k
27. Kelly, S. T.; Nigge, P.; Prakash, S.; Laskin, A.; Wang, B.; Tyliszczak, T.; Leone, S. R.; Gilles, M. K., An environmental sample chamber for reliable scanning transmission X-ray microscopy measurements under water vapor. *Rev. Sci. Instrum.* **2013,** *84*, 073708. DOI 10.10631/1.4816649

28. Steimer, S. S.; Lampimaki, M.; Coz, E.; Grzinic, G.; Ammann, M., The influence of physical state on shikimic acid ozonolysis: A case for in situ microspectroscopy. *Atmos. Chem. Phys.* **2014,** *14*, (19), 10761-10772. DOI 10.5194/Acp-14-10761-2014
29. Zelenay, V.; Ammann, M.; Krepelova, A.; Birrer, M.; Tzvetkov, G.; Vernooij, M. G. C.; Raabe, J.; Huthwelker, T., Direct observation of water uptake and release in individual submicrometer sized ammonium sulfate and ammonium sulfate/adipic acid particles using X-ray microspectroscopy. *J. Aerosol Sci.* **2011,** *42*, (1), 38-51. DOI 10.1016/j.jaerosci.2010.11.001
30. Zelenay, V.; Huthwelker, T.; Krepelova, A.; Rudich, Y.; Ammann, M., Humidity driven nanoscale chemical separation in complex organic matter. *Environ. Chem.* **2011,** *8*, (4), 450-460. DOI 10.1071/En11047
31. Ghorai, S.; Laskin, A.; Tivanski, A. V., Spectroscopic evidence of keto-enol tautomerism in deliquesced malonic acid particles. *J. Phys. Chem. A.* **2011,** *115*, (17), 4373-4380. DOI 10.1021/Jp112360x
32. Kilcoyne, A. L. D.; Tyliszczak, T.; Steele, W. F.; Fakra, S.; Hitchcock, P.; Franck, K.; Anderson, E.; Harteneck, B.; Rightor, E. G.; Mitchell, G. E.; Hitchcock, A. P.; Yang, L.; Warwick, T.; Ade, H., Interferometer-controlled scanning transmission X-ray microscopes at the Advanced Light Source. *J. Synchrotron. Radiat.* **2003,** *10*, 125-136. DOI 10.1107/S0909049502017739
33. Moffet, R. C.; Henn, T.; Laskin, A.; Gilles, M. K., Automated chemical analysis of internally mixed aerosol particles using X-ray spectromicroscopy at the carbon K-edge. *Anal. Chem.* **2010,** *82*, (19), 7906-7914. DOI 10.1021/Ac1012909
34. Henke, B. L.; Gullikson, E. M.; Davis, J. C., X-ray interactions -photoabsorption, scattering, transmission, and reflection at E=50-30,000 eV, Z=1-92. *Atom. Data Nucl. Data* **1993,** *54*, (2), 181-342. DOI 10.1006/Adnd.1993.1013
35. Zuend, A.; Marcolli, C.; Booth, A. M.; Lienhard, D. M.; Soonsin, V.; Krieger, U. K.; Topping, D. O.; McFiggans, G.; Peter, T.; Seinfeld, J. H., New and extended parameterization of the thermodynamic model AIOMFAC: calculation of activity coefficients for organic-inorganic mixtures containing carboxyl, hydroxyl, carbonyl, ether, ester, alkenyl, alkyl, and aromatic functional groups. *Atmos. Chem. Phys.* **2011,** *11*, (17), 9155-9206. Doi 10.5194/Acp-11-9155-2011
36. Zuend, A.; Marcolli, C.; Luo, B. P.; Peter, T., A thermodynamic model of mixed organic-inorganic aerosols to predict activity coefficients. *Atmos. Chem. Phys.* **2008,** *8*, (16), 4559-4593.
37. Cohen, M. D.; Flagan, R. C.; Seinfeld, J. H., Studies of concentrated electrolyte-solutions using the electrodynamic balance .3. Solute nucleation. *J. Phys. Chem.* **1987,** *91*, (17), 4583-4590. DOI 10.1021/J100301a031
38. Wise, M. E.; Biskos, G.; Martin, S. T.; Russell, L. M.; Buseck, P. R., Phase transitions of single salt particles studied using a transmission electron microscope with an environmental cell. *Aerosol. Sci. Tech.* **2005,** *39*, (9), 849-856. DOI 10.1080/02786820500295263
39. Mikhailov, E.; Vlasenko, S.; Martin, S. T.; Koop, T.; Pöschl, U., Amorphous and crystalline aerosol particles interacting with water vapor: conceptual framework and experimental evidence for restructuring, phase transitions and kinetic limitations. *Atmos. Chem. Phys.* **2009,** *9*, (24), 9491-9522.
40. Mochida, M.; Kawamura, K., Hygroscopic properties of levoglucosan and related organic compounds characteristic to biomass burning aerosol particles. *J. Geophys. Res.-Atmos.* **2004,** *109*, (D21), D21202. DOI 10.1029/2004jd004962

41. Kreidenweis, S. M.; Petters, M. D.; DeMott, P. J., Single-parameter estimates of aerosol water content. *Environ. Res. Lett.* **2008,** *3*, (3), Artn 035002. Doi 10.1088/1748-9326/3/3/035002
42. Petters, M. D.; Kreidenweis, S. M., A single parameter representation of hygroscopic growth and cloud condensation nucleus activity. *Atmos. Chem. Phys.* **2007,** *7*, (8), 1961-1971.
43. Tang, I. N., Thermodynamic and optical properties of mixed-salt aerosols of atmospheric importance. *J. Geophys. Res.-Atmos.* **1997,** *102*, (D2), 1883-1893. DOI 10.1029/96jd03085

Measuring Mass-Based Hygroscopicity of Atmospheric Particles through *in situ* Imaging

Dominique S. Piens,[1,#] Stephen T. Kelly,[1,%] Tristan H. Harder,[1,2] Markus D. Petters,[3] Rachel E. O'Brien,[1,&] Bingbing Wang,[4,^] Ken Teske,[5] Pat Dowell,[5] Alexander Laskin,[4] Mary K. Gilles[1,]*

[1]Chemical Sciences Division, Lawrence Berkeley National Laboratory, Berkeley, California 94720, USA

[2]Department of Chemistry, University of California, Berkeley, California 94720, USA

[3]Department of Marine Earth and Atmospheric Sciences, North Carolina State University, Raleigh, North Carolina 27695, USA

[4]William R. Wiley Environmental and Molecular Sciences Laboratory, Pacific Northwest National Laboratory, Richland, Washington 99352, USA

[5]Atmospheric Radiation Monitoring (Southern Great Plains Climate Research Facility, 109596 Coal Road, Billings, Oklahoma 74630 USA

[#]Present address: Stanford University, Stanford, California 94305, USA

[%]Present address: Carl Zeiss X-ray Microscopy Inc., Pleasanton, California 94588 USA

[&]Present address: Department of Civil and Environmental Engineering, Massachusetts Institute of Technology, Cambridge, Massachusetts 02139, USA

^Present address: College of Ocean and Earth Sciences, State Key Lab of Marine and Environmental Science, Xiamen University, Xiamen 361102, China

*E-mail: dpiens@stanford.edu

*Email: mkgilles@lbl.gov

STXM/NEXAFS Measurements

The presence of a specific element can be quantitatively *mapped* by comparing an image collected ~20 eV beyond the elemental absorption edge (post-edge) to an image collected at an energy ~5eV below that where the element absorbs (pre-edge). Similarly a molecular resonance, used for mapping chemical bonding, can be mapped by comparing an image obtained at the peak absorption to a pre-edge image. To quantify the presence of the functional group requires normalization to the total amount of the element present. This is done by using the difference between the post- and pre-edge images.

Carbon "short stacks" for subsequent analysis contained the following energies: three energies below the carbon K-edge (276 eV, 278 eV, and 280 eV); the C=C π* excitation (285.1 eV); 286.7 eV the C 1s → π* transition for carbon in a carboxylic acid (COOH) excitation (288.55 eV); the carbonate peak excitation (290.35 eV); and two energies above the carbon K-edge (318 eV, and 320 eV). Note the peak at 286.7 eV can arise from more than one potential transition: C 1s → π* in carbonyl-substituted aromatics and phenolic carbons attached to the OH group could have resonances at this energy (see Tivanski et al. 2007). The energies used to generate oxygen maps consisted of an energy below the oxygen K-edge (525 eV) as well as one above the oxygen K-edge (550 eV). Nitrogen mapping (discussed in a following section) was performed at the pre-edge (395 eV), the peak in the nitrogen absorption spectrum (406 eV), and post-edge (430 eV). Typically the nitrogen content is small and due to the long decaying tail of the carbon absorption, the post-edge value can be smaller than the pre-edge value. The result of this is that the total nitrogen absorption can be within the uncertainty of the measurement. Acquiring an image at the peak absorption typically has at least a factor of 3 higher contrast than the post-edge region, and enhances our ability to discern the presence of nitrogen.

Characterization of Southern Great Plains Samples

For characterization of the SGP dry samples, full stacks and short stacks (described above) were used. Briefly, the amount of EC, or sp^2 hybridized carbon can be quantified by comparing the absorption at the sp^2 peak (~285.4 eV) normalized for the total carbon to literature values for a highly oriented polycrystalline graphite (HOPG) standard. Based upon experiments with laboratory standards[22] and field samples,[14] we determined that a lower limit for soot content was obtained by using a threshold of 35% sp^2 content for EC. Organic carbon is identified using the COOH peak at 288.5 eV. The absorption at the carbon pre-edge (energies below where carbon absorb in the soft X-ray region) presumably originates from typical atmospheric inorganic species such as $(NH_4)_2SO_4$, NH_4NO_3, NaCl, and others. If the ratio of optical densities at the pre-edge and the post-edge is greater than 0.5, a pixel is assigned to non-carbonaceous inorganic matter.

Total Masses from STXM/NEXAFS and SEM/EDX: Atmospheric Particles of Unknown Composition

Nitrogen and silicon were not quantified in the SEM/EDX analysis because the SiNx substrate contains these elements. Nitrogen masses for the analyzed particles were measured using STXM/NEXAFS after the aerosol particles had undergone relative humidity cycling and SEM/EDX measurements. Although nitrogen typically accounts for a small (< 5%) fraction of total aerosol mass (Tivanski et al. 2007), STXM/NEXAFS analysis revealed a significant nitrogen contribution in these particular field collected aerosol particles. However, because these measurements were made after the SEM/EDX determination of the inorganic components (as well as post water vapor uptake experiments), the uncertainty is larger than if the nitrogen analysis had been performed on dry, unexposed samples.

The absolute uncertainty is estimated by comparing the nitrogen measured on particles previously analyzed using STXM/NEXAFS + SEM/EDX to proximal particles that were not previously subject to these analyses. The nitrogen masses of both groups of particles are of the same order of magnitude. Respectively, the mean and median nitrogen mass of previously analyzed particles are 47% lower and 42% higher than those of particles that had not been examined using SEM/EDX. It cannot be ruled out that the mass of nitrogen might have been altered by exposure to SEM/EDX + STXM/NEXAFS, but the conclusions of this manuscript and the validity of the methods presented are unaffected. Including the measured nitrogen masses in the mass-based growth factor calculations did not alter the clustering of the particles' water sorption isotherms. Moreover, growth factors that include nitrogen masses lead to average differences when compared with the previous growth factors that are below 2%, though the maximum difference is almost 14%. Since conclusions are only drawn from how particles cluster based on their growth factor, we are confident that the uncertainty due to nitrogen does not impact these results.

After establishing the uncertainty due to nitrogen, the uncertainty due to silicon was obtained by varying the atomic fraction of silicon within the inorganic elements from 0% to 100%. The maximal difference in growth factor, both with and without including nitrogen masses, was less than 0.4%. Hence, the uncertainty due to silicon is negligible. Figure 1 shows the mass-based growth factors of the field-collected particles with error bars representing the potential difference due to nitrogen and inorganic uncertainty. The uncertainty in the mass-based growth factor is mostly due to nitrogen, and therefore, not a concern for future applications of our methods that would measure nitrogen content prior to SEM/EDX and humidification experiments. Particles still group identically in terms of hygroscopic growth types, and mostly have the same ordering by mass-based growth factor. Observations on particles based on their type of hygroscopic growth are unaffected by uncertainties in nitrogen and inorganic content.

The size-based growth factors of the atmospheric particles yield very different growth curves and no obvious clustering. The size-based growth factor of a particle at a given RH is obtained by normalizing its size at that RH by its dry size. Here, size is measured by area equivalent diameter. In figure 2, retaining the same classification by type of hygroscopic growth obtained with mass-based growth factors shows that the ordering of the sorption isotherms changes when using size-based growth factors. Moreover, the ordering by size-based growth factor cannot be systematically mapped to the ordering by

mass-based growth factor. The findings in the manuscript could only result from relying on mass-based growth factors rather than size-based growth factors.

***In Situ* STXM/NEXAFS Water Vapor Uptake Measurements**.

The micro reactor of Kelly et al.[27] mounts directly into the STXM instruments at the Advanced Light Source. Advantages of the *in situ* reactor include: reduced absorption from the process gas (He with water vapor) by ~85% compared to filling the entire STXM chamber, the capacity to use a range of process gases, and enhanced image stability during data acquisition due to a decrease in thermal drift.[27] These advantages make it possible to acquire data over a large range of RH without sacrificing signal or spectral resolution.

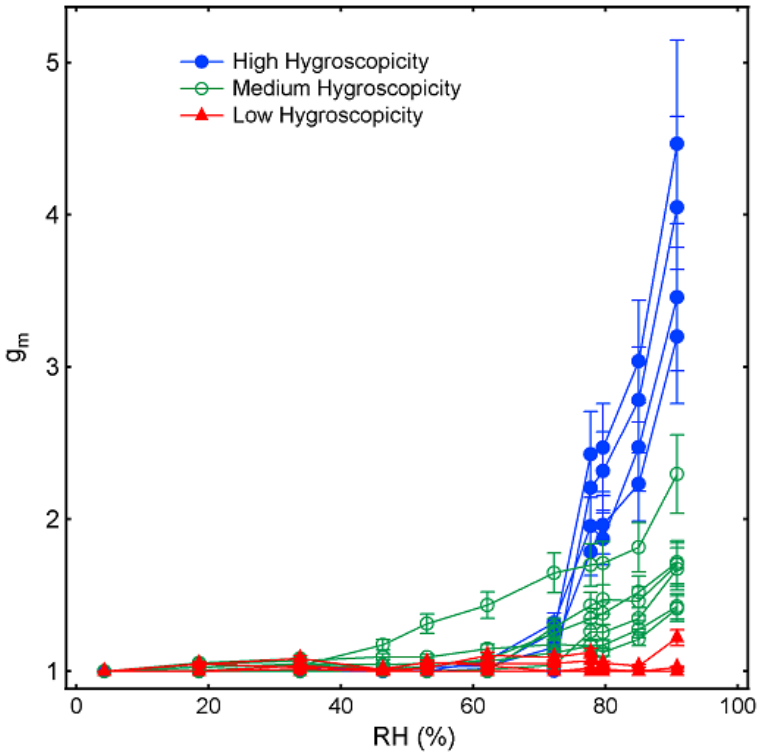

Figure S1. Mass-based growth factors for the 15 field-collected particles. Error bars represent the maximum difference due to including or removing nitrogen mass from total mass, as well as 20% differences in mass-absorption cross section.

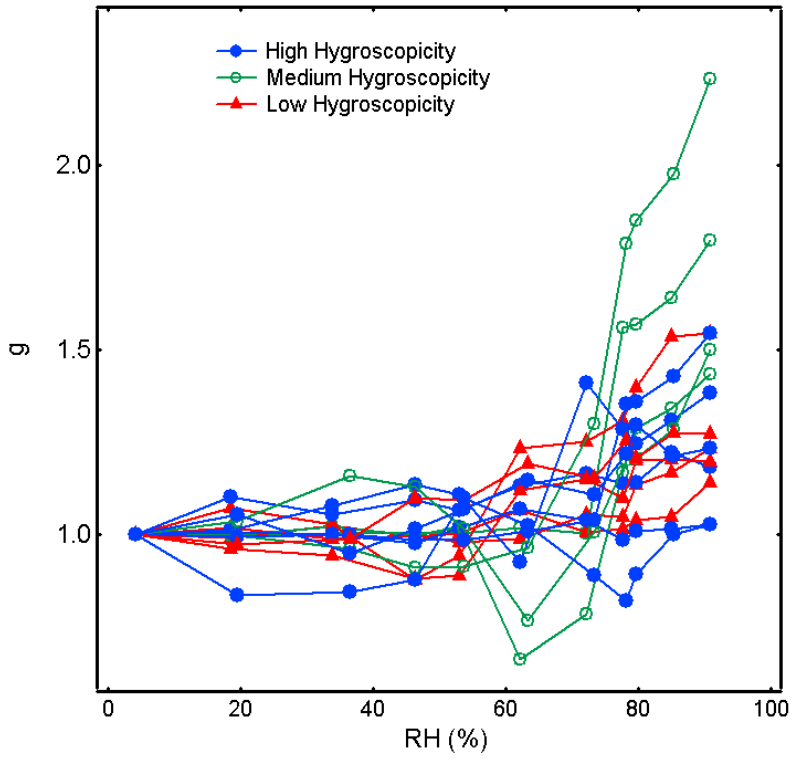

Figure S2. Size-based growth factors calculated using area equivalent diameters for the 15 field-collected particles.

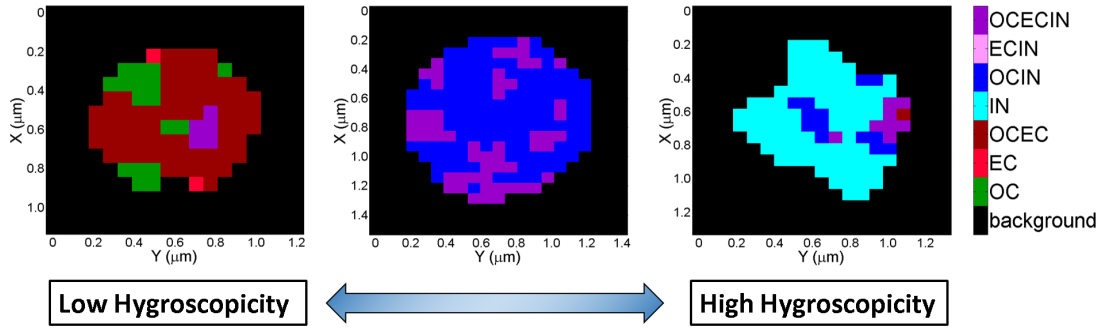

Figure S3. Correlation of mixing state and water uptake behavior. Each pixel was classified by its content of Inorganics (IN), Organic Carbon (OC) and Elemental Carbon (EC). A comparison to the water uptake behavior shows that a higher amount of inorganics is correlated to a higher uptake of water.

RESULTS AND DISCUSSION

Hygroscopic Behavior of Laboratory-Generated Samples with Known Composition

Table S1. Mass growth factors for sugars.

	Relative Humidity	Growth Factor, g_m	Standard Error	Number of Particles
Fructose	20	1.00	0.00	4
	40	1.15	0.06	4
	58	1.39	0.09	4
	74	1.73	0.11	4
	85	2.69	0.14	4
	91	3.09	0.12	4
	92	3.80	0.23	4
	93	4.04	0.19	4
Levoglucosan	4	1.00	0.00	3
	13	1.02	0.01	3
	26	1.06	0.00	2
	28	1.09	0.00	2
	47	1.18	0.01	2
	63	1.30	0.01	2
	77	1.67	0.14	3
	87	2.23	0.07	2
	93	3.54	0.17	2
	94	3.75	0.20	2

Table S2. Mass growth factors for $(NH_4)_2SO_4$.

	Relative Humidity	Growth Factor, g_m	Standard Error	Number of Particles
$(NH_4)_2SO_4$ (humidification)	6	1.00	0.00	4
	17	1.01	0.00	4
	29	1.00	0.00	4
	39	1.00	0.00	4
	51	1.01	0.01	4
	67	1.01	0.01	4
	70	1.02	0.01	4
	74	1.07	0.02	4
	77	2.27	0.04	4
$(NH_4)_2SO_4$ (dehumidification)	23	1.15	0.03	4
	30	1.34	0.04	4
	44	1.38	0.04	4
	49	1.48	0.04	4

Table S3. Mass growth factors for Halide Salts

	Relative Humidity	Growth Factor, g_m	Standard Error	Number of Particles
KCl (humidification)	6	1.30	0.12	4
	50	1.03	0.00	4
	64	1.03	0.00	4
	74	1.03	0.01	4
	79	1.33	0.12	4
	83	4.25	0.59	4
KCl (dehumidification)	64	2.27	0.49	4
	68	2.48	0.57	4
NaCl	8	1.04	0.00	6
	41	1.04	0.00	6
	47	1.04	0.01	6
	53	1.04	0.01	6
	59	1.05	0.01	6
	66	1.05	0.01	6
	67	1.05	0.01	6
	69	1.05	0.01	6
	71	1.04	0.00	3
	72	1.05	0.01	6
	73	1.07	0.00	3
	74	1.11	0.01	3

	74	3.43	0.65	3
NaBr	7	1.07	0.03	4
	31	1.07	0.03	4
	35	1.04	0.02	4
	37	1.08	0.03	4
	39	1.02	0.01	4
	41	1.07	0.03	4
	43	1.04	0.02	4
	45	1.08	0.03	4
	47	1.09	0.02	4
	49	1.61	0.09	4
	58	2.01	0.03	4
	70	2.50	0.17	4
	78	3.59	0.35	4

Hygroscopic Behavior of Atmospheric Aerosol Samples of Unknown Composition

Table S4. Mass growth factors for low hygroscopicity particles presented in Figure 2.

Relative Humidity	**Particle 1**	**Particle 2**	**Particle 3**	**Particle 4**	**Particle 5**
4	1.00	1.00	1.00	1.00	1.00
19	1.00	1.00	1.06	1.00	1.06
34	1.04	1.00	1.10	1.02	1.03
46	1.01	1.01	1.01	1.00	1.02
53	1.03	1.00	1.07	1.00	1.07
62	1.12	1.00	1.04	1.00	1.06

72	1.11	1.00	1.00	1.00	1.06
78	1.15	1.00	1.02	1.00	1.08
80	1.02	1.00	1.00	1.00	1.07
85	1.00	1.00	1.00	1.00	1.04
91	1.00	1.00	1.03	1.00	1.27

Table S5. Mass growth factor for medium hygroscopicity particles presented in Figure 2.

Relative Humidity	**Particle 1**	**Particle 2**	**Particle 3**	**Particle 4**	**Particle 5**	**Particle 6**
4	1.00	1.00	1.00	1.00	1.00	1.00
19	1.03	1.05	1.06	1.00	1.03	1.01
34	1.06	1.08	1.10	1.00	1.06	1.04
46	1.05	1.11	1.00	1.01	1.01	1.21
53	1.06	1.11	1.00	1.00	1.04	1.38
62	1.08	1.18	1.00	1.01	1.09	1.52
72	1.15	1.21	1.35	1.05	1.30	1.78
78	1.20	1.20	1.52	1.31	1.41	1.84
80	1.15	1.21	1.57	1.31	1.46	1.85
85	1.25	1.33	1.55	1.42	1.62	1.98
91	1.49	1.51	1.84	1.81	1.86	2.56

Table S6. Mass growth factors for high hygroscopicity particles presented in Figure 2.

Relative Humidity	**Particle 1**	**Particle 2**	**Particle 3**	**Particle 4**
4	1.00	1.00	1.00	1.00
19	1.00	1.00	1.00	1.00
34	1.02	1.00	1.02	1.00
46	1.00	1.00	1.00	1.02
53	1.03	1.00	1.00	1.00
62	1.04	1.00	1.02	1.08
72	1.19	1.00	1.31	1.38
78	1.94	2.44	2.71	2.14
80	2.15	2.57	2.76	2.04
85	2.48	3.13	3.44	2.76
91	3.64	4.65	5.15	3.94

Table S7. Inorganic atomic fractions for low, medium, and high hygroscopicity particles shown in Figure 3.

	Low Hygroscopicity		Medium Hygroscopicity		High Hygroscopicity	
Element	**Mean Fraction (%)**	**Standard Deviation**	**Mean Fraction (%)**	**Standard Deviation**	**Mean Fraction (%)**	**Standard Deviation**
Al	12.91	6.84	8.99	2.92	9.42	0.99
Ca	11.55	6.98	10.15	5.46	4.18	1.54
Cl	11.84	4.44	9.20	2.83	14.23	2.08
Fe	4.16	2.73	3.57	1.56	4.43	0.63
K	2.70	0.91	3.03	0.94	3.89	0.42
Mg	8.31	5.89	12.00	5.10	7.00	1.24
Mn	1.68	1.35	1.47	0.63	3.20	2.44
Na	11.69	3.18	11.61	1.67	18.90	3.94
P	7.62	9.09	4.93	2.54	8.46	2.06
S	15.97	11.14	25.70	6.79	13.81	5.36
Zn	3.26	4.38	1.47	0.99	2.05	1.46

Table S8. Mixing state classification in Figure 4.

	158 Representative Particles			15 particles for H_2O uptake		
Mixing state	**Number of particles**	**Upper error**	**Lower error**	**Number of particles**	**Upper error**	**Lower error**
OC	16	7	3	0	0	0
OCIN	33	4	7	6	1	2
OCEC	41	3	7	1	0	0
OCECIN	68	8	4	8	2	1

Table S9. Area equivalent diameter classification in Figure 4.

	158 Representative Particles			15 particles for H_2O uptake		
Area Equivalent Diameter (μm)	**Number of particles**	**Upper error**	**Lower error**	**Number of particles**	**Upper error**	**Lower error**
0.0-0.5	8	13	7	1	1	1
0.5-1.0	85	5	18	8	1	0
1.0-1.5	53	16	14	5	0	2
1.5-2.0	9	9	1	0	1	0
>2.0	3	0	3	1	0	1